

Chemical Science

Accepted Manuscript



This article can be cited before page numbers have been issued, to do this please use: Y. Zeng, M. Wang, W. He, P. Fang, M. Wu, Y. Tong, M. Chen and X. Lu, *Chem. Sci.*, 2019, DOI: 10.1039/C8SC04967J.



This is an Accepted Manuscript, which has been through the Royal Society of Chemistry peer review process and has been accepted for publication.

Accepted Manuscripts are published online shortly after acceptance, before technical editing, formatting and proof reading. Using this free service, authors can make their results available to the community, in citable form, before we publish the edited article. We will replace this Accepted Manuscript with the edited and formatted Advance Article as soon as it is available.

You can find more information about Accepted Manuscripts in the [author guidelines](#).

Please note that technical editing may introduce minor changes to the text and/or graphics, which may alter content. The journal's standard [Terms & Conditions](#) and the ethical guidelines, outlined in our [author and reviewer resource centre](#), still apply. In no event shall the Royal Society of Chemistry be held responsible for any errors or omissions in this Accepted Manuscript or any consequences arising from the use of any information it contains.

Journal Name

COMMUNICATION

Engineering High Reversibility and Fast Kinetics of Bi Nanoflakes by Surface Modulation for Ultrastable Nickel-Bismuth Batteries

 Yinxiang Zeng,^a Mengying Wang,^a Wanyi He,^a Pingping Fang,^a Mingmei Wu,^{*a} Yexiang Tong,^a Minghua Chen,^{*b} and Xihong Lu^{*a,b}

 Received 00th January 20xx,
Accepted 00th January 20xx

DOI: 10.1039/x0xx00000x

www.rsc.org/

The exploration of stable and high-rate anode is of pivotal importance for achieving advanced aqueous rechargeable batteries. Owing to the beneficial properties of high conductivity, suitable negative working voltage, and three-electron redox, bismuth (Bi) is considered as promising anode material, but it suffers from the poor stability. Here, we successfully endow Bi nanoflakes (NFs) with prominent cycling performance by one-step surface oxidation approach to remarkably boost its reversibility. As a result, the partially oxidized Bi NFs (BiO_x) show admirable capacity (0.38 mA h cm⁻² at 2 mA cm⁻²), good rate capability and superior long-term stability (almost no capacity decay after 20000 cycles). Furthermore, a durable aqueous Ni//Bi battery is constructed based on the optimized BiO_x anode, which exhibits excellent durability with 96% capacity retention after 5000 cycles. This study could open a new avenue for the rational design of efficient anodes for eco-friendly and reliable aqueous rechargeable batteries.

Introduction

Economical, environmentally friendly, and reliable energy storage devices are critical for the widespread utilization of renewable-but-intermittent energy sources.¹⁻⁵ Among numerous candidates, aqueous rechargeable batteries (ARBs) have sparked extensive scientific interest owing to their intrinsically good safety, high ionic conductivities (~ 1 S cm⁻¹) and cost effectiveness.⁶⁻⁹ In particular, aqueous rechargeable Ni//Zn batteries, which feature high output voltage (~1.8 V), good rate capability, materials abundance and eco-friendliness, represent a compelling class of new energy storage device.¹⁰⁻¹³ For instance, Dai and his coworkers

reported an ultrafast rechargeable Ni//Zn battery based on deposited Zn anode, which delivered a high capacity of 0.307 mA h cm⁻² and retained about 90% of initial capacity after 600 cycles.¹¹ Additionally, an aqueous yarn-shape NiCo//Zn battery using Zn nanoflakes (NFs) anode achieved a high areal capacity of ~0.17 mA h cm⁻² at 5 mA cm⁻², together with decent durability (60% capacity retention after 1000 cycles).¹⁴ Despite these notable progress, the lifespan of most reported rechargeable Ni//Zn battery is insufficient due to the irreversible reaction and dendrite formation of the Zn anode, diminishing the commercial competitive advantages of Ni//Zn batteries.^{12, 15} Hence, exploiting a new reliable and alternative anode with high reversibility as well as excellent stability is extremely desirable for long-life ARBs, yet remains a formidable challenge.

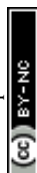
Bismuth-based materials have held great promise as desired anodes for ARBs owing to their environmentally friendliness, favorable negative working window in aqueous electrolyte, and fast 3-electrons redox reaction.¹⁶⁻¹⁸ To date, a variety of nanostructured bismuth-based materials including bismuth (Bi),^{16, 19} Bi₂O₃,^{6, 17} Bi₂O₃/graphene,¹⁸ (BiO)₄CO₃(OH)₂,²⁰ etc. have been explored and showed impressive performance. Among them, Bi with its inherently metallic characteristic and low molecular weight nature presents particular advantages, favoring higher conductivity and theoretical capacity (384.8 mAh g⁻¹).^{16, 19} Bi film was investigated to afford a capacity of 0.055 mA h cm⁻² and 40% capacity attenuation after 90 cycles.¹⁹ Based on Bi hierarchical nanostructured anode, a NiCo₂O₄//Bi battery was firstly reported to exhibit a maximum energy density of 1.52 mW h cm⁻³ and 89% capacity retention over 1000 cycles.¹⁶ Although significant achievement having been gained, the most obstacles of those Bi electrodes for actual application are their unsatisfactory cycling durability and capacity, particularly at high mass loading (> 3.0 mg cm⁻²).

To tackle these issues, herein we demonstrate an efficient and general surface oxidation strategy to effectively boost the stability and capacity of Bi NFs by enhancing the electrochemical reaction reversibility. Bi electrode is acknowledged to proceed a redox reaction in alkaline media (2Bi⁰ + 6OH⁻ - 6e⁻ ⇌ Bi₂O₃ + 3H₂O).¹⁶ It is speculated that the adsorption property of OH⁻ ion on the Bi surface has vital effect on its redox reaction since OH⁻ takes part in the redox

^a MOE of the Key Laboratory of Bioinorganic and Synthetic Chemistry, The Key Lab of Low-carbon Chem & Energy Conservation of Guangdong Province, School of Chemistry, Sun Yat-Sen University, Guangzhou 510275, China, E-mail: luxh6@mail.sysu.edu.cn; ceswmm@mail.sysu.edu.cn

^b Key Laboratory of Engineering Dielectric and Applications (Ministry of Education), Harbin University of Science and Technology, Harbin 150080, China E-mail: mhchen@hrbust.edu.cn

Electronic Supplementary Information (ESI) available: [details of any supplementary information available should be included here]. See DOI: 10.1039/x0xx00000x



reaction.²¹ To discover the OH⁻ ion absorption on the surface of electrode, density functional theory (DFT) calculation is applied as a guide before the experiments. As shown in Fig. 1a, the absorption energy of OH⁻ ion for Bi with the introduction of oxygen atoms on its surface (-3.71 eV) is much lower than that of pristine Bi (-3.42 eV), indicating that Bi with the introduction of oxygen atoms has much stronger and easier capability for adsorbing OH⁻ ions. It is anticipated that the surface oxidation of Bi could enhance its absorption capability for OH⁻ ion, thus improving the electrochemical performance of the Bi electrode. Electrochemical results reveal that the partially oxidized Bi NFs (denoted as BiO_x) prepared by a facile controllable oxidation technique show unprecedented long-term cycling performance with negligible capacity decay after even 20000 cycles, remarkably superior to the pristine Bi NFs (42.6% capacity retention). Moreover, by virtue of rich active sites and fast electron/ion transport ability, the BiO_x NF electrode also owns a high areal capacity (0.38 mA h cm⁻² at 2 mA cm⁻²) and an extraordinary rate capability. Additionally, based on this BiO_x anode, a robust and stable aqueous Ni//Bi battery is demonstrated, achieving a high energy density of 3.66 mW h cm⁻³ and outstanding cyclability (4% capacity attenuation after 5000 cycles), outperforming most currently reported ARBs.

Results and Discussion

The partially oxidized Bi NFs were synthesized by a two-step process. Firstly, the Bi NFs on carbon cloth were prepared by a facile electrodeposition approach with a potential of -0.8 V for 20 min (details in the Experimental Section). Scanning electron microscopy (SEM) images (Fig. S1) reveal that the surface of each carbon fiber are covered uniformly with Bi NFs without any binder, ensuring a favorable pathway for electron transfer and ion diffusion. After surface oxidation by a controllable successive water oxidation method (Experimental Section), no obvious morphological change can be noticed for the BiO_x NFs (Fig. 1b). Further structural features were investigated via the transmission electron microscopy (TEM) analysis of the BiO_x NFs (Fig. 1c), in which a lattice fringe with d-spacing of 0.328 nm can be indexed to the (012) planes of metal Bi (JCPDS (Joint Committee on Powder Diffraction Standards) #44-1246). Another interplanar spacing of 0.319 nm matches well with the d₂₀₁ spacing of Bi₂O₃ (JCPDS #65-1209), implying the coexistence of metallic Bi and Bi₂O₃ in hybrid BiO_x NF sample. And the thickness of Bi₂O₃ is about 8-13 nm. In contrast, only lattice fringe spacings of 0.328 and 0.395 nm corresponding to Bi (JCPDS #44-1246) can be detected for the pristine Bi sample (Fig. S2). The corresponding energy-dispersive spectroscopy (EDS) mapping images of the BiO_x NF sample clearly verify the homogeneous spatial distribution of Bi and O elements (Fig. 1d). Moreover, the atomic force microscopy (AFM) image in Fig. 1e and the corresponding height profile (Fig. 1f) of the BiO_x sample depict a single NF with an average thickness of ~7.5 nm.

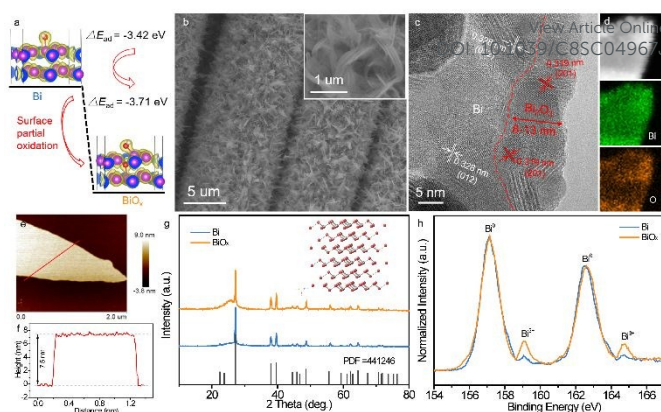


Fig. 1 (a) The calculated adsorption free energy changes of OH⁻ on the pristine Bi and Bi with the introduction of oxygen atoms. (b) SEM image (c) TEM image (the red ring region presents the Bi₂O₃) (d) EDS mapping of the BiO_x NFs. (e) AFM image of the BiO_x NFs and (f) the corresponding height profiles measured for Line in (e). (g) XRD patterns (h) Bi 4f XPS spectra of the Bi and BiO_x NFs.

More evidence for the pristine Bi and BiO_x samples was confirmed by XRD and Raman analysis. As shown in Fig. 1g, except for the peak from carbon cloth, all the diffraction peaks for both samples fit well with the characteristic peaks of hexagonal Bi (JCPDS #44-1246), indicating the high purity of the metallic Bi. Furthermore, Raman spectra illustrate that two peaks located at 68.4 and 94.3 cm⁻¹ for both samples can be assigned to the E_g and A_{1g} fundamental modes of metallic Bi, respectively (Fig. S3).^{16, 22} There are no other signals of Bi₂O₃ or other bismuth oxides detected for BiO_x sample in XRD or Raman spectra, which may be ascribed to the low content of oxygen. To further investigate the surface oxidation state of the pristine Bi and BiO_x samples, X-ray photoelectron spectroscopy (XPS) measurement was conducted. Fig. 1h compares the core level Bi 4f XPS spectra of the pristine Bi and BiO_x samples, where the peaks centered at 157.1 and 162.5 eV can be indexed to the typical 4f_{7/2} and 4f_{5/2} peaks of Bi⁰, respectively, and the peaks at 159.1 and 164.7 eV correspond to the characteristic peaks of Bi³⁺.^{17, 23} Evidently, the pristine Bi is almost entirely composed of Bi⁰, but the BiO_x sample presents higher fractions of Bi existing in the Bi³⁺ state, again suggesting the partial oxidation of metallic Bi for BiO_x sample.

The electrochemical properties of the Bi electrodes were evaluated in a three-electrode system with 1 M KOH as aqueous electrolyte. The cyclic voltammetry (CV) curves of the pristine Bi and BiO_x electrodes show that two well-defined reduction peaks and oxidation peaks are distinctly identified with little distortion from 1 to 20 mV s⁻¹ (Fig. S4), confirming the good electrochemical behavior and highly reversible redox reaction of both electrodes. The two cathodic and anodic peaks may correspond to the two-step reaction in KOH electrolyte described as following: Bi⁰ - e⁻ ⇌ Bi⁺; 6Bi⁺ + 6OH⁻ ⇌ Bi₂O₃ + 3H₂O + 4Bi⁰.¹⁶ Encouragingly, the polarization between oxidation and reduction peak in CV curve for the BiO_x electrode is visibly lower than that for the pristine Bi electrode (Fig. 2a), suggesting improved reversibility of the Bi electrode after surface oxidation. To gain insight into the difference in charge storage kinetics between the pristine Bi and BiO_x electrodes, log *i* (current density) versus log *v* (scan rate) of the anodic and cathodic peaks for both electrodes was plotted, and all emerge nearly straight lines (Fig.



S5). Specifically, the b value determined from the slope of cathodic peak for both electrodes is 0.51, meaning that the cathodic current is almost controlled by semi-infinite diffusion. While the b values of anodic peak for pristine Bi and BiO_x electrodes are 0.76 and 0.87, respectively, suggesting the corresponding redox reactions at the peak regions of BiO_x electrode is more affected by capacitive processes.

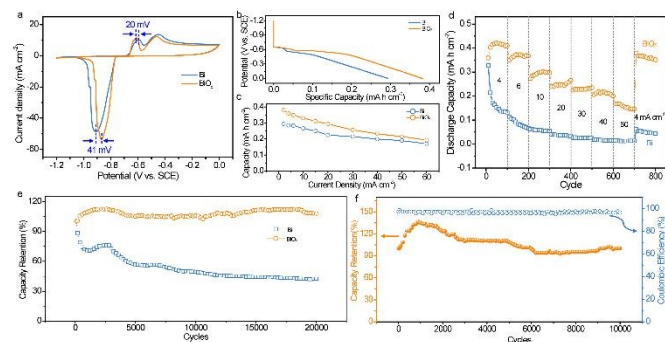


Fig. 2 (a) CV curves at 4 mV s^{-1} , (b) discharge curves at 2 mA cm^{-2} , (c) areal capacitance as a function of discharge current density, and (d) rate performance at various current densities of the Bi and BiO_x electrodes. (e) Cycling performance of the Bi and BiO_x electrodes for 20000 cycles at 100 mV s^{-1} . (f) Cycling performance and coulombic efficiency of the BiO_x electrode at 40 mA cm^{-2} .

Fig. 2b compares the discharge profiles of the pristine Bi and BiO_x electrodes at a current density of 2 mA cm^{-2} . The BiO_x electrode delivers lower and longer discharge voltage plateaus than that of the pristine Bi electrode, implying its better electrochemical performance. At 2 mA cm^{-2} , a remarkable areal capacity of $0.38 \text{ mA h cm}^{-2}$ is achieved by the BiO_x electrode, obviously higher than that of the pristine Bi electrode ($0.29 \text{ mA h cm}^{-2}$) and other previously documented anodes for ARBs.^{16, 17, 24} To highlight, more than 50% capacity retention could be still maintained even at an ultrahigh current density of 60 mA cm^{-2} (Fig. 2c, S6), which demonstrates its extraordinary rate capability. The rate performance of the BiO_x electrode is a little inferior than that of the pristine Bi owing to the increased charge transfer resistance (R_{ct}) after oxidation, which can be verified by the Nyquist plots (Fig. S7). Within the current densities ranging from 2 to 60 mA cm^{-2} , the capacities of the BiO_x electrode are always higher than these values obtained for the pristine Bi electrode, indicating the electrochemical property of Bi is considerably boosted upon surface oxidation. The good rate property of the BiO_x electrode is further revealed in Fig. 2d, in which as the current density increases stepwise from 4 to 60 mA cm^{-2} , the discharge capacities are 0.358 and $0.167 \text{ mA h cm}^{-2}$, respectively. Meanwhile, as the current density switches back to 4 mA cm^{-2} , a significant capacity of $0.362 \text{ mA h cm}^{-2}$ is retained after over 800 cycles at various current densities, revealing its excellent stability and reversibility of the redox reactions during intense current fluctuation. In contrast, the pristine Bi displays a much poorer cycling performance than those of BiO_x electrode. At a current density of 4 mA cm^{-2} , the pristine Bi presents an initial capacity of $0.327 \text{ mA h cm}^{-2}$, but decreases to only $0.045 \text{ mA h cm}^{-2}$ after 800 cycles.

The unprecedented long-term durability is the most appealing property of the BiO_x electrode. As depicted in Fig. 2e, the capacity of BiO_x electrode remains nearly unchanged after even 20000 cycles,

while only 42.6% capacity retention is preserved by the pristine Bi electrode. This value also outperforms most recently reported anodes for ARBs or supercapacitors (SCs), such as Bi_2O_3 (74.5% after 200 cycles),⁶ $r\text{-Bi}_2\text{O}_3/\text{GN}$ (90% after 1000 cycles),¹⁸ $\text{CNTs}/\text{Fe}_2\text{O}_3$ (96% after 1000 cycles),²⁴ VOS@C (92.3% after 10000 cycles),²⁵ $\text{N-Fe}_2\text{O}_3$ (95.2% after 10000 cycles),²⁶ hierarchical Bi nanostructures (96% after 10000 cycles).¹⁶ SEM observations of the pristine Bi and BiO_x electrodes after cycling illustrated that both electrodes started to change after 5 cycles and underwent marked changes in morphology after 20 cycles derived from repeated redox reaction between Bi and Bi^{3+} (Fig. S8, S9). Specifically, the pristine Bi underwent huge morphology change for the first 50 cycles than the BiO_x sample, indicative of more structural damage for the pristine Bi for the first several cycles. Inductively coupled plasma emission spectroscopy (ICP) analysis gives more detailed evidence. As shown in Fig. S10, the Bi concentration in electrolyte after 20000 cycles for BiO_x electrode is lower than that of the pristine Bi electrode, confirming that the surface oxidation of Bi electrode could mitigate the dissolution issue in KOH electrolyte. Furthermore, the cycle life of the BiO_x electrode was further investigated at a high current density of 40 mA cm^{-2} (Fig. 2f). Significantly, the BiO_x electrode can maintain about 100% of its original capacity and over 95% Coulombic efficiency after charging-discharging 10000 cycles, manifesting again its excellent cycling property. In addition, the influence of the oxidation degree on the cyclic stability of Bi was also studied. From XPS analysis, the ratio of O to Bi of pristine Bi increased sharply from 0.54 to 2.12 after surface oxidation for 25 cycles and then increased steadily to 2.15, 2.21, 2.29 for 50, 100, 200 cycles of oxidation (Figure S11a). Calculated by thermogravimetry results, the ratio of Bi_2O_3 to Bi is 0.21, 0.23, 0.27, 0.33, respectively for the BiO_x -25, BiO_x -50, BiO_x -100, BiO_x -200 electrodes (Figure S11b). Above all, the oxidation degree increased gradually with the increment of ALD cycles. Indeed, surface oxidation of Bi could remarkably improve its cycle life in some extent and Bi sample with 50 cycles of oxidation achieved the optimal performance (Fig. S12). Besides, surface oxidation of Bi electrode has little effect on its areal capacity (Fig. S13).

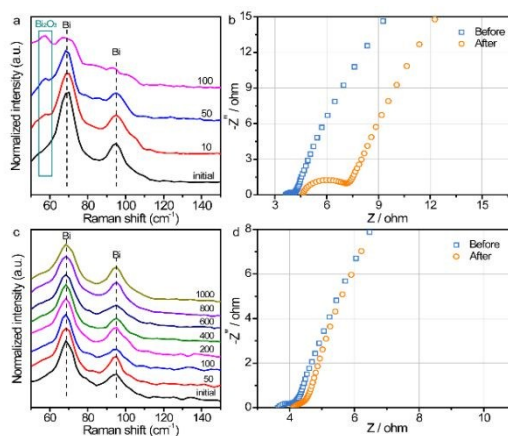


Fig. 3 (a) Raman spectra at different cycles and (b) Nyquist plots collected before and after cycling of Bi electrode. (c) Raman spectra at different cycles and (d) Nyquist plots collected before and after cycling of BiO_x electrode.

To further elucidate the possible reasons for the enhanced cyclability of BiO_x electrode, the chemical component changes of the



Bi and BiO_x electrodes during cycling process were monitored by *in situ* Raman spectroscopy. Fig. 3a displays the Raman spectra of the pristine Bi sample after certain cycles of charging-discharging process. Obviously, the intensity of the characteristic Bi_2O_3 Raman peak ($\sim 55 \text{ cm}^{-1}$) emerges and increases gradually, while the peaks for metallic Bi weakening slightly after only 100 cycles, evidencing the formation of Bi_2O_3 derived from the irreversible reaction of pristine Bi during repeated cycling. By comparison, the Raman spectra for BiO_x sample remain almost unchanged with two sharp metallic Bi peaks even after 1000 cycles (Fig. 3c), indicative of a highly reversible redox reaction of the BiO_x sample. Fig. S14 compares the Raman spectra of the pristine Bi and BiO_x electrodes after 20000 cycle life. The cycled pristine Bi electrode exhibits Raman peaks assigned to Bi_2O_3 , which is absent for the cycled BiO_x electrode, implying again the irreversible oxidation of the pristine Bi during cycling.²² Additionally, the ratios of O to Bi for the pristine Bi and BiO_x samples after certain cycles were evaluated by energy-dispersive spectroscopy (EDS) measurement (Table S1). The ratios of O to Bi for pristine Bi electrode increased gradually during the cycling process and reached 1.21 after 10000 cycles, suggesting the formation of bismuth oxide during charging-discharging process, in good agreement with Raman result. In contrast, the ratios of O to Bi for BiO_x electrode presented little increment even after 10000 cycles, showing a reversible reaction for BiO_x electrode. EIS was carried out to further elaborate the effect of charging-discharging process on electronic properties. From Nyquist plots of the pristine Bi (Fig. 3b), the R_{ct} increased substantially after 20000 cycles, which can explain the severe capacity decay of the pristine Bi. While for the BiO_x electrode, the R_{ct} before and after 20000 cycles are almost consistent (Fig. 3d), confirming its pronounced long-term stability during repetitive charging-discharging, in line with the Raman analysis. SEM images for the BiO_x electrode after ultrasounding for 1h further verify that BiO_x NFs are adhered tightly and strongly to the carbon cloth substrate (Fig. S15) Based on above results, the remarkably boosted electrochemical performance of the BiO_x electrode is ascribed to the reasons that (1) the OH^- adsorption ability of Bi could be improved after surface oxidation, further increasing its electrochemical performance; (2) the BiO_x electrode could effectively prevent the excessive oxidation of Bi during charging-discharging process, contributing to enhanced reversibility; (3) the strategy of surface oxidation is able to mitigate the dissolution and capacity decay of Bi electrode during charging-discharging process; (4) the strong adhesive strength between BiO_x NFs and carbon fiber surface, enabling these NFs not easy to fall off during the charging/discharging process. We further implemented this strategy by annealing the pristine Bi sample in air to assess its feasibility. As expected, the pristine Bi annealed at 200 °C for 5 min presented striking long-term cyclability with nearly no capacity decay after 20000 cycles (Fig. S16), which is consistent with the BiO_x electrode. In contrast, the Bi electrode annealed under N_2 atmosphere at 200 °C for 5 min exhibited much inferior cycling stability with 58.2% capacity retention after 20000 cycles. Therefore, this proposed surface oxidation strategy holds great promise to be applicable to improve the cycling performance of Bi.

With high rate capability and outstanding lifespan, the BiO_x electrode shows great promise as advanced anode for high-power and reliable ARBs. Thus, a nickel-bismuth battery consisting of BiO_x anode and Ni-NiO cathode was constructed (denoted as Ni//Bi

battery). The Ni-NiO cathode was prepared via electroplating Ni on carbon cloth and subsequent oxidation process (details are given in the Experimental Section and Supporting Information). SEM images showed that a rugged Ni-NiO film was coated tightly on the surface of carbon cloth (Fig. S17a). XRD pattern in Fig. S17b presented that all peaks were indexed well with the metallic Ni (JCPDS # 65-2845), which might be ascribed to the slightly low content of NiO. Electrochemical test revealed that as-prepared Ni-NiO electrode is a promising cathode in KOH electrolyte (Fig. S18). Fig. S19a comparatively depicts the CV curves of the Ni-NiO cathode and BiO_x

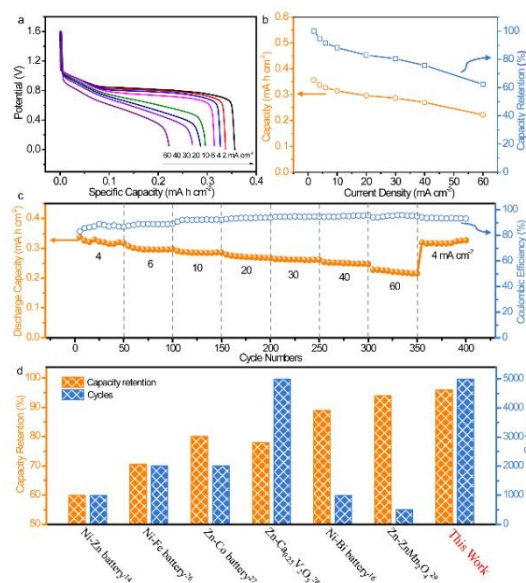


Fig. 4 (a) Discharge curves at various current densities, (b) areal capacity and capacity retention, (c) cycling performance and coulombic efficiency at various current density of the as-fabricated Ni//Bi battery. (d) Cycling performance comparison of the Ni//Bi battery with previous studies.^{14, 16, 27-30}

anode at 50 mV s^{-1} , in which both electrodes present well-defined redox peaks. The CV profiles of the Ni//Bi battery with different operating potential demonstrate a suitable voltage window of 1.6 V (Fig. S19b). As shown in Fig. S19c, the CV curves of the Ni//Bi battery own similar shapes even at a high scan rate of 100 mV s^{-1} , revealing its fast and reversible charge storage capability. Additionally, the representative galvanostatic discharge curves of the Ni//Bi battery at various current densities were displayed in Fig. 4a and all have noticeable discharge plateaus. More importantly, the Ni//Bi battery delivered a strikingly high capacity of 0.356 mA h cm^{-2} at current density of 2 mA cm^{-2} , surpassing most recently reported ARBs, such as aqueous NiCo_2O_4 //Bi battery (0.08 mA h cm^{-2} at 1 mA cm^{-2}),¹⁶ Zn// Co_3O_4 battery (0.153 mA h cm^{-2} at 2.1 mA cm^{-2}),³¹ Li ion battery (0.157 mA h cm^{-2} at 1 mA cm^{-2}),³² $\text{H}_2\text{V}_3\text{O}_8$ //Zn battery (0.289 mA h cm^{-2} at 1.2 mA cm^{-2}).³³ Moreover, a superb rate capability has been realized by this Ni//Bi battery, with 62.3% capacity retention when the current density raised to 60 mA cm^{-2} (Fig. 4b).

The rate performance of the Ni//Bi battery is further investigated at a series of current densities ranging from 4 to 60 mA cm^{-2} (Fig. 4c). The Ni//Bi battery exhibits discharge capacities of 0.338, 0.307, 0.29, 0.278, 0.263, 0.254, 0.227 mA h cm^{-2} at 4, 6, 10, 20, 30,



40, 60 mA cm⁻², respectively. When the current density was returned to 4 mA cm⁻², the discharge capacity recovered to 0.319 mA h cm⁻² with a recovery ratio of 94.4%, suggesting the Ni//Bi battery owns fast reaction kinetics and excellent high rate performance. The prolonged cycling performance of the Ni//Bi battery at high rate (40 mA cm⁻²) was illustrated in Fig. S20. Encouragingly, an impressive capacity retention of 96% together with high Coulombic efficiency approaching 100% were accomplished by the Ni//Bi battery over 5000 cycles, substantially outstripping most current ARBs (Fig. 4d, Table S1).^{14, 16, 27-30}

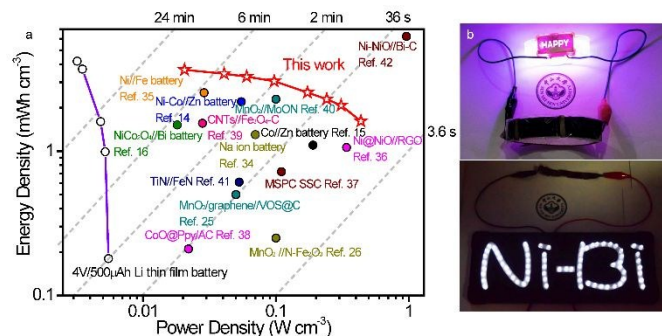


Fig. 5 (a) Ragone plots of the Ni//Bi battery, with the comparison of the recently developed other energy storage devices.^{14-16, 25, 26, 34-42} (b) Pictures showing an LED indicator powered by the tandem Ni//Bi battery.

The energy density and power density of the Ni//Bi battery relative to existing ARBs and SCs were evaluated using Ragone plots. As plotted in Fig. 5a, our fabricated Ni//Bi battery delivered a highest volumetric energy density of 3.66 mWh cm⁻³, which is considerably higher than that of the reported ARBs and SCs.^{14, 16, 26, 34, 35} A remarkable volumetric power density of 0.436 W cm⁻³ was also achieved by the Ni//Bi battery, together with high energy density of 1.61 mWh cm⁻³, even much higher than most SCs.^{37, 39, 41} With comparable energy density to commercial Li thin film battery, our fabricated Ni//Bi battery generates ~ 4-80 times higher power density, suggesting its superfast charge-discharge ability.^{27, 42} To visually illustrate the potential of this Ni//Bi battery for practical applications, three prototype devices in series were employed to power a 3 V “Ni-Bi” shape light-emitting diode (LED) indicators and LED lights of a wristwatch effectively (Fig. 5b).

Conclusions

To summarize, a facile strategy of one-step surface oxidation was reported to significantly enhance the durability of Bi NFs. By improving the reaction reversibility, the optimized BiO_x electrode possessed outstanding cyclic life with almost unattenuated capacity even after 20000 cycles. Moreover, the BiO_x NF electrode with sufficient active sites delivered a remarkable areal capacity of 0.38 mA h cm⁻² at 2 mA cm⁻² as well as favorable rate capability (0.19 mA h cm⁻² at 60 mA cm⁻²). Capitalizing on the as-prepared BiO_x NF anode, we assembled a high performance aqueous Ni//Bi battery, affording excellent durability with 96% capacity retention after 5000 cycles. Furthermore, a maximum energy density of 3.66 mWh cm⁻³ was achieved by the Ni//Bi battery, together with a high power density of 0.436 W cm⁻³, surpassing most recently reported ARBs. The efficient

surface oxidation strategy could provide a certain reference to the relevant materials.

DOI: 10.1039/C8SC04967J

Conflicts of interest

There are no conflicts to declare.

Acknowledgements

This work was financially supported by the National Natural Science Foundation of China (21822509, U1810110, 31530009 and 51672315), Guangdong Natural Science Funds for Distinguished Young Scholar (2014A030306048), Tip-top Scientific and Technical Innovative Youth Talents of Guangdong Special Support Program (2015TQ01C205), Pearl River Nova Program of Guangzhou (201610010080), the Science and Technology Planning Project of Guangzhou City for International Cooperation Program (20170430020). We also thank the Photoemission Endstations (BL10B) in National Synchrotron Radiation Laboratory (NSRL) for help in characterizations.

Notes and references

- F. Wan, L. Zhang, X. Dai, X. Wang, Z. Niu and J. Chen, *Nat. Commun.*, 2018, **9**, 1656.
- J. Zhou, Z. Jiang, S. Niu, S. Zhu, J. Zhou, Y. Zhu, J. Liang, D. Han, K. Xu, L. Zhu, X. Liu, G. Wang and Y. Qian, *Chem*, 2018, **4**, 372-385.
- Y. Zhong, X. Xia, S. Deng, J. Zhan, R. Fang, Y. Xia, X. Wang, Q. Zhang and J. Tu, *Adv. Energy Mater.*, 2018, **8**, 1701110.
- H. Hu, C. Shi, K. Guo, T. Zhai, H. Li and Y. Wang, *Angew. Chem. Int. Ed.*, 2018, **57**, 8214-8218.
- M. Song, H. Tan, D. Chao and H. J. Fan, *Adv. Funct. Mater.*, 2018, **28**, 1802564.
- W. Zuo, W. Zhu, D. Zhao, Y. Sun, Y. Li, J. Liu and X. W. Lou, *Energy Environ. Sci.*, 2016, **9**, 2881-2891.
- X. Wu, Y. Qi, J. J. Hong, Z. Li, A. S. Hernandez and X. Ji, *Angew. Chem. Int. Ed.*, 2017, **56**, 13026-13030.
- F. Wang, O. Borodin, T. Gao, X. Fan, W. Sun, F. Han, A. Faraone, J. A. Dura, K. Xu and C. Wang, *Nat. Mater.*, 2018, **17**, 543-549.
- J. Huang, Z. Wang, M. Hou, X. Dong, Y. Liu, Y. Wang and Y. Xia, *Nat. Commun.*, 2018, **9**, 2906.
- J. F. Parker, C. N. Chervin, I. R. Pala, M. Machler, M. F. Burz, J. W. Long and D. R. Rolison, *Science*, 2017, **356**, 415-418.
- M. Gong, Y. Li, H. Zhang, B. Zhang, W. Zhou, J. Feng, H. Wang, Y. Liang, Z. Fan, J. Liu and H. Dai, *Energy Environ. Sci.*, 2014, **7**, 2025-2032.
- J. Liu, C. Guan, C. Zhou, Z. Fan, Q. Ke, G. Zhang, C. Liu and J. Wang, *Adv. Mater.*, 2016, **28**, 8732-8739.
- Y. Zeng, Z. Lai, Y. Han, H. Zhang, S. Xie and X. Lu, *Adv. Mater.*, 2018, **30**, 1802396.
- Y. Huang, W. S. Ip, Y. Y. Lau, J. Sun, J. Zeng, N. S. S. Yeung, W. S. Ng, H. Li, Z. Pei, Q. Xue, Y. Wang, J. Yu, H. Hu and C. Zhi, *ACS Nano*, 2017, **11**, 8953-8961.
- M. Li, J. Meng, Q. Li, M. Huang, X. Liu, K. A. Owusu, Z. Liu and L. Mai, *Adv. Funct. Mater.*, 2018, **28**, 1802016.
- Y. Zeng, Z. Lin, Y. Meng, Y. Wang, M. Yu, X. Lu and Y. Tong, *Adv. Mater.*, 2016, **28**, 9188-9195.
- H. Xu, X. Hu, H. Yang, Y. Sun, C. Hu and Y. Huang, *Adv. Energy Mater.*, 2015, **5**, 1401882.

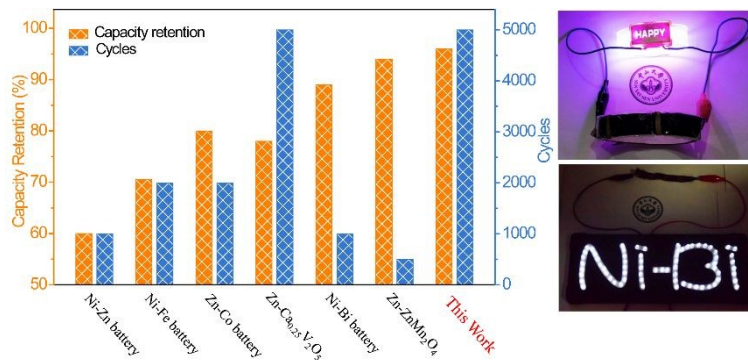


18. R. Liu, L. Ma, G. Niu, X. Li, E. Li, Y. Bai and G. Yuan, *Adv. Funct. Mater.*, 2017, **27**, 1701635.
19. W. Zuo, P. Xu, Y. Li and J. Liu, *Nanomater.*, 2015, **5**, 1756-1765.
20. J. Sun, J. Wang, Z. Li, L. Niu, W. Hong and S. Yang, *J. Power Sources*, 2015, **274**, 1070-1075.
21. Q. Zhang, M. D. Levi, Q. Dou, Y. Lu, Y. Chai, S. Lei, H. Ji, B. Liu, X. Bu, P. Ma and X. Yan, *Adv. Energy Mater.*, 2018, DOI: 10.1002/aenm.201802707.
22. K. Trentelman, *J. Raman. Spectrosc.*, 2009, **40**, 585-589.
23. P. Zhang, Y. Zeng, M. Wang, W. Xu, Y. Liu and X. Lu, *J. Mater. Chem. A*, 2018, **6**, 8895-8900.
24. J. Liu, M. Chen, L. Zhang, J. Jiang, J. Yan, Y. Huang, J. Lin, H. J. Fan and Z. X. Shen, *Nano Lett.*, 2014, **14**, 7180-7187.
25. T. Zhai, X. Lu, Y. Ling, M. Yu, G. Wang, T. Liu, C. Liang, Y. Tong and Y. Li, *Adv. Mater.*, 2014, **26**, 5869-5875.
26. X. Lu, Y. Zeng, M. Yu, T. Zhai, C. Liang, S. Xie, M. S. Balogun and Y. Tong, *Adv. Mater.*, 2014, **26**, 3148-3155.
27. C. Guan, W. Zhao, Y. Hu, Q. Ke, X. Li, H. Zhang and J. Wang, *Adv. Energy Mater.*, 2016, **6**, 1601034.
28. X. Wang, F. Wang, L. Wang, M. Li, Y. Wang, B. Chen, Y. Zhu, L. Fu, L. Zha, L. Zhang, Y. Wu and W. Huang, *Adv. Mater.*, 2016, **28**, 4904-4911.
29. C. Xia, J. Guo, P. Li, X. Zhang and H. N. Alshareef, *Angew. Chem. Int. Ed.*, 2018, **57**, 3943-3948.
30. N. Zhang, F. Cheng, Y. Liu, Q. Zhao, K. Lei, C. Chen, X. Liu and J. Chen, *J. Am. Chem. Soc.*, 2016, **138**, 12894-12901.
31. L. Ma, S. Chen, H. Li, Z. Ruan, Z. Tang, Z. Liu, Z. Wang, Y. Huang, Z. Pei, J. A. Zapien, C. Zhi, *Energy Environ. Sci.*, 2018, **11**, 2521-2530.
32. X. Dong, L. Chen, J. Liu, H. Servane, Y. Wang, Y. Xia, *Sci. Adv.*, 2016, **2**, e1501038.
33. P. He, Y. Quan, X. Xu, M. Yan, W. Yang, Q. An, L. He and L. Mai, *Small*, 2017, **13**, 1702551.
34. S. Dong, L. Shen, H. Li, G. Pang, H. Dou and X. Zhang, *Adv. Funct. Mater.*, 2016, **26**, 3703-3710.
35. H. Wang, Y. Liang, M. Gong, Y. Li, W. Chang, T. Mefford, J. Zhou, J. Wang, T. Regier, F. Wei and H. Dai, *Nat. Commun.*, 2012, **3**, 917.
36. R. Li, Y. Wang, C. Zhou, C. Wang, X. Ba, Y. Li, X. Huang and J. Liu, *Adv. Funct. Mater.*, 2015, **25**, 5384-5394.
37. M. Yu, D. Lin, H. Feng, Y. Zeng, Y. Tong and X. Lu, *Angew. Chem. Int. Ed.*, 2017, **56**, 5454-5459.
38. M. Yu, X. Cheng, Y. Zeng, Z. Wang, Y. Tong, X. Lu and S. Yang, *Angew Chem Int Ed Engl*, 2016, **55**, 6762-6766.
39. M. Yu, W. Wang, C. Li, T. Zhai, X. Lu and Y. Tong, *NPG Asia Mater.*, 2014, **6**, e129.
40. C. Zhu, P. Yang, D. Chao, X. Wang, X. Zhang, S. Chen, B. K. Tay, H. Huang, H. Zhang, W. Mai and H. J. Fan, *Adv. Mater.*, 2015, **27**, 4566-4571.
41. C. Zhou, Y. Zhang, Y. Li and J. Liu, *Nano Lett.*, 2013, **13**, 2078-2085.
42. Y. Zeng, Z. Lin, Z. Wang, M. Wu, Y. Tong and X. Lu, *Adv. Mater.*, 2018, **30**, 1707290.

View Article Online
DOI: 10.1039/C8SC04967J



Table of Contents



An efficient and facile surface partial oxidation strategy was demonstrated to significantly enhance the reversibility and durability of Bi nanoflakes.

